NANO LETTERS

Letter

pubs.acs.org/NanoLett

Probing the Role of Interlayer Coupling and Coulomb Interactions on Electronic Structure in Few-Layer $MoSe_2$ Nanostructures

Aaron J. Bradley,[†,▲] Miguel M. Ugeda,*[,†,▲] Felipe H. da Jornada,[†,‡,▲] Diana Y. Qiu,[†,‡] Wei Ruan,[†,§] Yi Zhang,[∥,⊥] Sebastian Wickenburg,[†,‡] Alexander Riss,[†,¶] Jiong Lu,[†,∇,#] Sung-Kwan Mo,[∥] Zahid Hussain,[∥] Zhi-Xun Shen,[⊥,■] Steven G. Louie,[†,‡] and Michael F. Crommie*[,†,‡,○]

[†]Department of Physics, University of California at Berkeley, Berkeley, California 94720, United States

[‡]Materials Sciences Division, Lawrence Berkeley National Laboratory, Berkeley, California 94720, United States

[§]State Key Laboratory of Low Dimensional Quantum Physics, Department of Physics, Tsinghua University, Beijing 100084, China

[∥]Advanced Light Source, Lawrence Berkeley National Laboratory, Berkeley, California 94720, United States

[⊥]Stanford Institute for Materials and Energy Sciences, SLAC National Accelerator Laboratory, Menlo Park, California 94025, United States

[∇]Centre for Advanced 2D Materials and Graphene Research Centre, National University of Singapore, 6 Science Drive 2, Singapore 117546, Singapore

[■]Geballe Laboratory for Advanced Materials, Departments of Physics and Applied Physics, Stanford University, Stanford, California 94305, United States

[○]Kavli Energy NanoSciences Institute, University of California Berkeley and the Lawrence Berkeley National Laboratory, Berkeley, California 94720, United States

S *Supporting Information*

ABSTRACT: Despite the weak nature of interlayer forces in transition metal dichalcogenide (TMD) materials, their properties are highly dependent on the number of layers in the few-layer two-dimensional (2D) limit. Here, we present a combined scanning tunneling microscopy/spectroscopy and GW theoretical study of the electronic structure of high quality single- and few-layer $MoSe_2$ grown on bilayer graphene. We find that the electronic (quasiparticle) bandgap, a fundamental parameter for transport and optical phenomena, decreases by nearly one electronvolt when going from one layer to three due to interlayer coupling and screening effects. Our results paint a clear picture of the evolution of the electronic wave function hybridization in the valleys of both the valence and conduction bands as the number of layers is changed. This demonstrates the importance of layer number and electron−electron interactions on van der Waals heterostructures and helps to clarify how their electronic properties might be tuned in future 2D nanodevices.

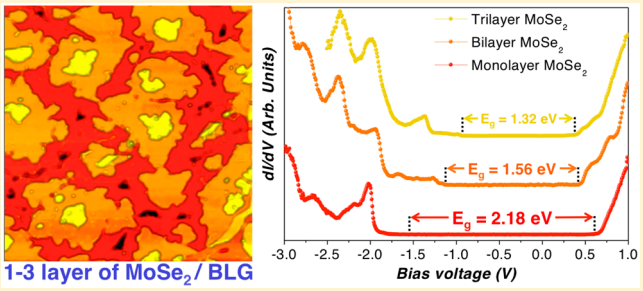

KEYWORDS: *transition metal dichalcogenide, graphene, quasiparticle bandgap, Coulomb interaction, screening, STM/STS*

Owing to their inherently 2D nature, few-layer semiconducting TMDs exhibit a number of unique physical attributes that are extremely sensitive to the number of layers.[1−6] This provides new opportunities for creating van der Waals heterostructures with tailored properties and designed functionalities. For example, few-layer TMDs have been shown to support larger current densities than single layer electronic nanodevices,[7] and the photovoltaic response of p−n junctions has been shown to be sensitive to the number of TMD layers.[8] Despite the promise of few-layer TMDs for electronic and optoelectronic applications; there is so far little understanding of how the overall electronic structure evolves with layer number close to the 2D limit. Most previous spectroscopic studies of few-layer TMD semiconductors have been via optical measurements[9−13] that only indirectly measure bandstructure, as well as photoemission[14,15] studies that primarily focus on states near the Fermi energy and in the valence band. Although many theoretical studies have been performed,[16−21] a consistent picture has not yet emerged and many critical parameters, such as bandgaps and conduction band structure, remain ambiguous. In the present combined STM/STS/theory study of few-layer $MoSe_2$ on bilayer graphene, we characterize how the electronic bandgap (E_g), the valence band local density of states (LDOS), *and* the conduction band LDOS change with the number of $MoSe_2$ layers between 1 (monolayer (ML)), 2

Received: January 14, 2015
Revised: March 10, 2015
Published: March 16, 2015

DOI: 10.1021/acs.nanolett.5b00160
Nano Lett. 2015, 15, 2594−2599

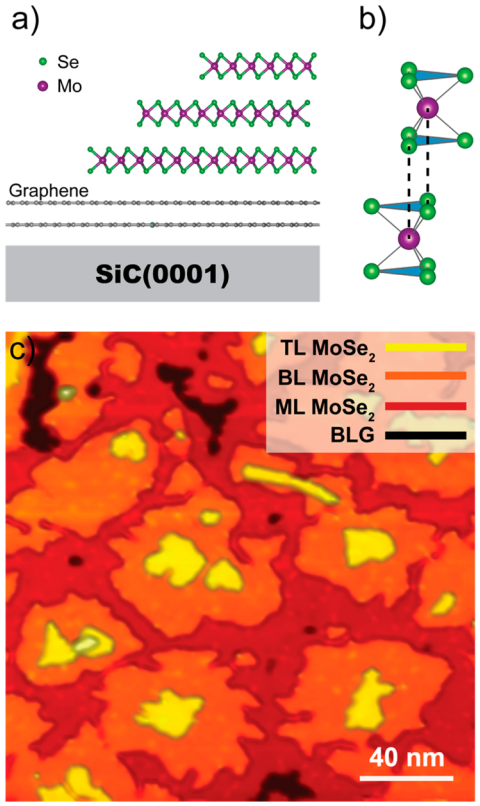

Figure 1. (a) Sketch of few-layer $MoSe_2$. Se atoms are shown in green, whereas Mo atoms are in purple. (b) 2H stacking configuration of $MoSe_2$ with both the Se and the Mo atoms in an AB1 stacking pattern (see Supporting Information for more details). (c) Typical STM image of 1.4 monolayer $MoSe_2$/BLG (V_{bias} = +1.5 V, I_t = 30 pA, T = 5 K).

(bilayer (BL)), and 3 (trilayer (TL)). These measurements compare favorably with *ab initio* GW calculations, revealing the important influence of interlayer coupling and Coulomb interactions on these properties, as well as the relative contributions from different parts of the Brillouin zone.

Low temperature (5 K) STM/STS experiments were carried out on high quality $MoSe_2$ grown on bilayer graphene (BLG) on 6H-SiC(0001) substrates via molecular beam epitaxy.[14] A sketch of the structure of few-layer $MoSe_2$ is shown in Figure 1a. Figure 1b depicts the 2H stacking arrangement for $MoSe_2$, which we have confirmed in this study based on comparison between experiment and theory (see Supporting Information for a detailed discussion of the stacking). Samples grown with an average $MoSe_2$ coverage ranging between 0.8 and 2 ML exhibit coexisting regions of ML, BL, and TL $MoSe_2$, as well as bare BLG substrate, as shown in the STM image of Figure 1c. Though the TL regions in Figure 1c are relatively small compared with the ML and BL regions, we are able to tune the sizes of the different layered regions by altering the $MoSe_2$ coverage. This allowed us to maximize the area of ML, BL, or TL regions and to avoid confinement and edge effects in our STS measurements.

Variations in the electronic structure between ML, BL, and TL $MoSe_2$ films on BLG were experimentally determined via STS using standard lock-in techniques[6] (all STS data were acquired at least 5 nm away from step edges, defects, and domain boundaries). Figure 2a–c show typical STM dI/dV spectra for ML, BL, and TL $MoSe_2$, respectively. Each spectrum reveals a relatively wide bandgap surrounded by features in both the valence and conduction bands. Prominent features that determine the band edges (V_1, C_1), as well as newly discovered features in the conduction band (C_1, C_2), are marked in the spectra. Bandgap values were determined by

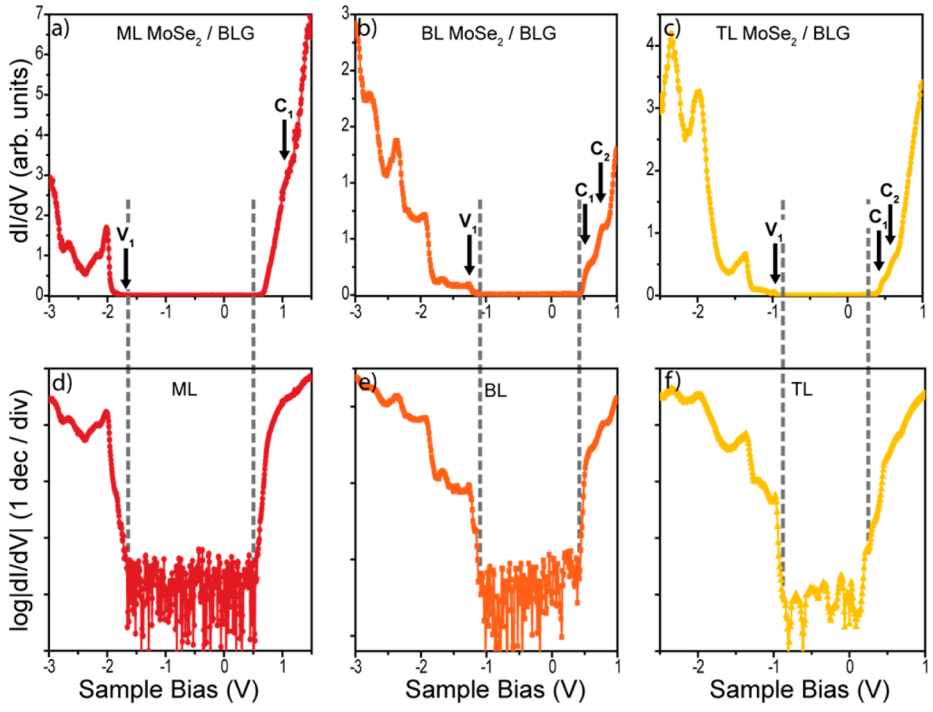

Figure 2. Representative STS spectra (T = 5 K) obtained for (a) ML $MoSe_2$/BLG (lock-in wiggle voltage: ΔV_{rms} = 4 mV, f = 872 Hz, set point current: I_t = 5 nA), (b) BL $MoSe_2$/BLG (lock-in wiggle voltage: ΔV_{rms} = 5 mV, f = 871 Hz, set point current: I_t = 100pA), and (c) TL $MoSe_2$/BLG (lock-in wiggle voltage: ΔV_{rms} = 5 mV, f = 871 Hz, set point current: I_t = 5 nA). (d–f) Same STS curves shown on a logarithmic scale to highlight the electronic band edges (band edges are marked by dashed lines).

DOI: 10.1021/acs.nanolett.5b00160
Nano Lett. 2015, 15, 2594–2599

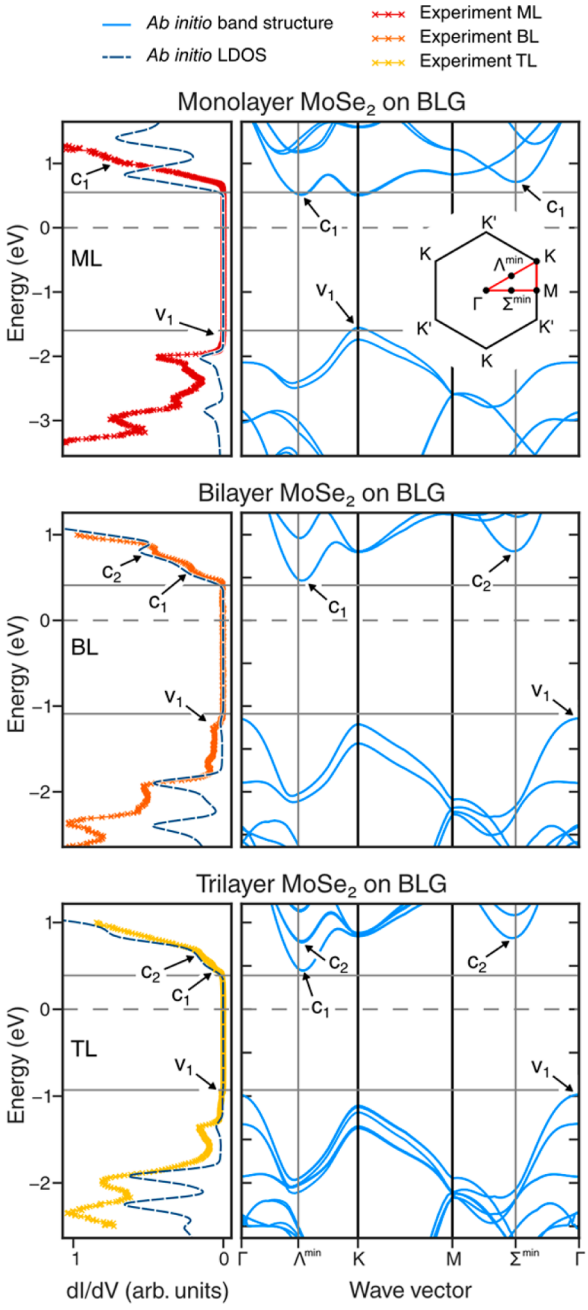

Figure 3. Right panels: *ab initio* GW band structure of ML, BL, and TL $MoSe_2$, including screening effects from the BLG substrate. Left panels: corresponding simulated LDOS (dashed blue lines) along with experimental STM d*I*/d*V* spectra for ML (dark red), BL (orange), and TL (yellow) $MoSe_2$. The horizontal solid lines mark the experimental VBM and CBM, and the dashed lines denote the experimental Fermi energy.

examining the d*I*/d*V* spectra on a logarithmic scale (Figure 2d–f) and following the statistical analysis procedure described in ref 6. For ML, BL, and TL $MoSe_2$/BLG we determine bandgap values of $E_{g,ML}$ = 2.18 ± 0.04 eV, $E_{g,BL}$ = 1.56 ± 0.04 eV, $E_{g,TL}$ = 1.32 ± 0.04 eV, respectively. Uncertainty in the values of E_g arises mainly due to lateral spatial inhomogeneity and tip-induced band bending.[6,22] Lateral inhomogeneity causes band edges to rigidly shift by 10s of meV from point to point in both the bilayer and trilayer, whereas lateral variations in ML $MoSe_2$ are smaller by an order of magnitude.

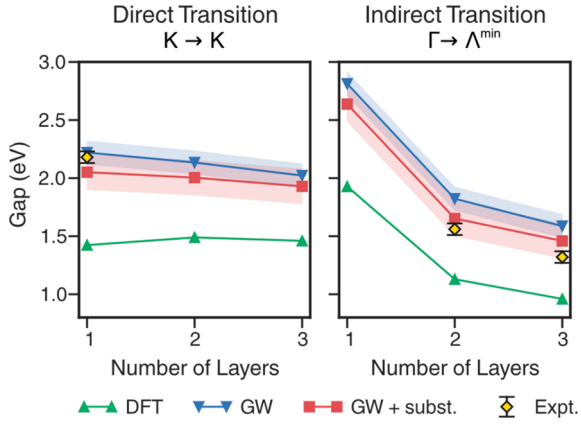

Figure 4. Direct and indirect bandgaps for few-layer $MoSe_2$ calculated within different levels of theory (triangles and squares) and obtained from experimental STS measurements (diamonds). The shaded regions mark the theoretical uncertainty in the GW calculations (see Supporting Information). All levels of theory predict a crossover from direct to indirect bandgap as the number of layers is increased from one to two. The theoretical uncertainty arises primarily due to the GW approximation of the electronic self-energy and the approximate treatment of the substrate (see Supporting Information).

These rigid shifts are presumably due to inhomogeneous doping effects and do not significantly affect the measured energy gap values. The position of the Fermi energy (V_{bias} = 0 V) with respect to the band edges indicates that these samples have very low n-type doping.

In order to interpret our experimental results, we performed *ab initio* simulations of the quasiparticle electronic structure of ML, BL, and TL $MoSe_2$. These simulations allowed us to systematically study how the electronic structure of few-layer $MoSe_2$ is affected by the following factors: (1) different multilayer stacking configurations; (2) many-electron interactions; (3) interactions with the substrate; and (4) the spatial distribution of electronic states. We start by discussing the role of the stacking configuration. Five possible stacking configurations exist for two layers of $MoSe_2$. Three of these have an inversion center and two do not. We performed density functional theory (DFT) simulations for all five stacking configurations and determined that the stacking labeled AB1 (Figure 1b) is the correct stacking sequence based on both its calculated stability and its match with experimentally observed spectroscopic features (see Supporting Information for more details). All calculations for BL and TL $MoSe_2$ were therefore performed using the AB1 structure.

Many-electron interactions were included in our calculations through the *ab initio* GW technique[23] as implemented using the BerkeleyGW package[24] (this was necessary because bare DFT does not yield accurate quasiparticle energies[23] nor optical transition energies[25]). In the first stage of the calculations, we intentionally neglected the effect of the substrate by considering free-standing ML, BL, and TL $MoSe_2$. In order to speed the convergence with respect to k-point sampling, we employed nonuniform sampling of the Brillouin zone, where the smallest q-vector corresponds to ∼1/1150th of a reciprocal lattice vector (more details in Supporting Information). To address the role of the substrate we then calculated the effect of a doped bilayer graphene substrate on supported few-layer $MoSe_2$ (the SiC was ignored because it is much less polarizable than BLG and is further away from the $MoSe_2$ layers). BLG screening of

DOI: 10.1021/acs.nanolett.5b00160
Nano Lett. 2015, 15, 2594–2599

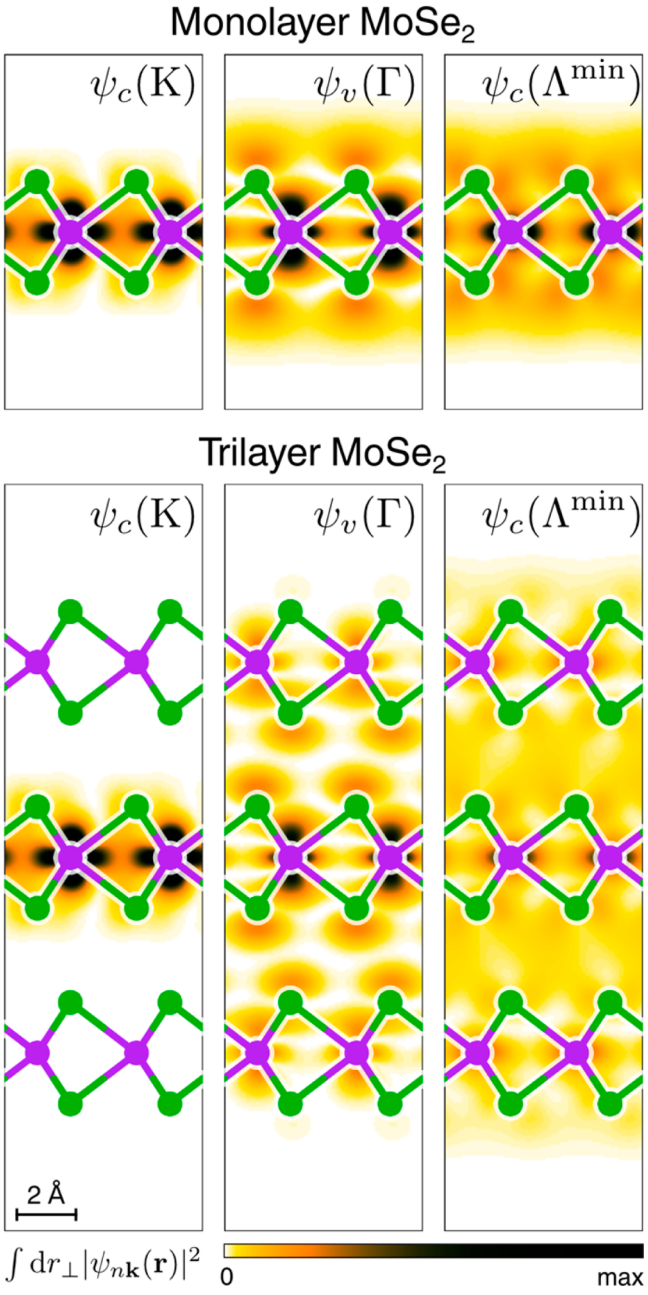

Figure 5. Modulus squared of calculated electronic wave functions for different Bloch states for ML and TL $MoSe_2$. The horizontal axis follows the [110] direction (same as Figure 1a), the vertical axis points in the out-of-plane direction, and the wave functions have been integrated in the direction perpendicular to the page. Se atoms are shown in green, whereas Mo atoms are in purple.

the $MoSe_2$ layers was calculated following the same method as in ref 6.

The final calculated quasiparticle band structure (including screening contributions from the BLG substrate) for ML, BL, and TL $MoSe_2$ is plotted in the right panels of Figure 3. This electronic structure was used to compute the LDOS above the $MoSe_2$ surface which gives a measure of the STM differential conductance (dI/dV) within the Tersoff-Hamann approximation[26] with no adjustable parameters (see Supporting Information for technical details). These theoretical STM dI/dV simulations are compared with the experimental STS spectra in the left panels of Figure 3. We observe good agreement between the theoretical LDOS and the experimental dI/dV curves, especially near the valence band maxima (VBM) and conduction band minima (CBM). This procedure allows us to identify the reciprocal-space origin of the experimental features V_1, C_1, and C_2 in Figure 2 by calculating the contributions of different regions of the Brillouin zone (see Supporting Information for more details). We are thus able to conclude that the experimental valence band feature V_1 originates from the K point for the ML and from the Γ point for the BL and TL structures. The experimental conduction band features C_1 and C_2 are seen to arise from near the Λ^{min} and Σ^{min} points of reciprocal space, where Λ^{min} is the point halfway between Γ and K, and Σ^{min} is the point halfway between Γ and M (see inset in Figure 3). The general good agreement between theory and experiment, especially for features close to the VBM and CBM, provides strong evidence that the main features seen in the experimental STS spectra come from the intrinsic electronic structure of $MoSe_2$ and not from extrinsic effects (such as defect states).

A comparison of our experimental and theoretical bandgaps for few-layer $MoSe_2$ can be seen in Figure 4. The most accurate calculated bandgaps (taking into account both GW and substrate corrections) for the ML, BL, and TL structures are 2.05 ± 0.15 eV, 1.65 ± 0.15 eV, and 1.46 ± 0.15 eV, respectively—within the experimental error bars. Though the magnitude of the calculated gap varies significantly with theoretical formalism, all levels of theory predict that monolayer $MoSe_2$ is a direct bandgap material at the K point of the Brillouin zone, whereas BL and TL $MoSe_2$ have indirect gaps spanning Γ_v to Λ_c^{min} (in contrast to some predictions that the indirect gap spans Γ_v to K_c[14,16]). These indirect transitions are also corroborated by the experimental dI/dV curves because the valence band edge signal is stronger in the BL and TL structures than in the ML structure, indicating that the valence band edge is closer to the Γ point in BL and TL $MoSe_2$ (see V_1 features in Figures 2a–c). From our calculations, the effect of the substrate reduces the direct energy gaps inhomogeneously in reciprocal space (not shown), affecting states near Γ more than states near K. In all cases, the substrate plays a decreasing role as the number of layers is increased.

We are able to gain further insight into the electronic structure of few-layer $MoSe_2$ by examining how the spatial dependence of the simulated electronic states changes with layer number. Figure 5 shows the modulus squared of ML and TL wave functions at the K, Γ, and Λ^{min} points in the bandstructure. The major contribution to the conduction band state at K (ψ_C(K) upper left panel) is from the Mo d orbital, so it is not expected to hybridize significantly as we add more layers. Indeed, the corresponding state ψ_C(K) in the TL structure (lower left panel) looks very similar to the ML state. The valence states at K (not shown) also display little hybridization, and so we may conclude that the direct bandgap at K would not be significantly affected by hybridization between different layers. This picture is consistent with the fact that the direct gap at K predicted by DFT is constant with the number of layers (green line in Figure 4, left panel). The picture is different for the indirect gap. The highest valence state at Γ ($\psi_V(\Gamma)$) in ML $MoSe_2$ (upper middle panel in Figure 5) has a significant contribution from Se p orbitals that are able to interact with similar orbitals on Se atoms in adjacent layers. Indeed, the corresponding state $\psi_V(\Gamma)$ in TL $MoSe_2$ (lower middle panel) displays significant hybridization. The lowest conduction band state at Λ^{min} ($\psi_C(\Lambda^{min})$) is qualitatively

DOI: 10.1021/acs.nanolett.5b00160
Nano Lett. 2015, 15, 2594–2599

different in the degree to which it is highly delocalized. This state is strongly modified as its spatial confinement is decreased by going from the ML to the TL structure (right panels). These differences in the character of the $\psi_V(\Gamma)$ and $\psi_C(\Lambda^{min})$ states are responsible for driving the direct-to-indirect transition in $MoSe_2$ as layer the number is increased.

In conclusion, we have measured the electronic structure of semiconducting $MoSe_2$ as a function of layer number for monolayer, bilayer, and trilayer stacking. We find that the addition of layers in the 2-dimensional regime causes the electronic bandgap to significantly shrink in size while simultaneously creating new features in both the valence and conduction bands. These experimental results are explained with theoretical GW calculations that take into account stacking geometry, wave function hybridization, electron−electron interactions, and substrate screening, thus providing new insight into how different electronic structure features arise from Bloch state properties within the Brillouin zone. The deeper understanding gained here into the electronic properties of few-layer TMD materials should help in the creation of next-generation 2D nanodevices.

■ ASSOCIATED CONTENT

Supporting Information

Finding bilayer stacking configuration, theoretical dI/dV calculation, electronic structure calculations. This material is available free of charge via the Internet at http://pubs.acs.org.

■ AUTHOR INFORMATION

Corresponding Authors

*E-mail: mmugeda@berkeley.edu.
*E-mail: crommie@berkeley.edu.

Present Addresses

[¶]Institute of Applied Physics, Vienna University of Technology, Wiedner Hauptstr. 8-10/134, 1040 Wien, Austria.
[#]Centre for Advanced 2D Materials and Graphene Research Centre, National University of Singapore, 6 Science Drive 2, Singapore 117546, Singapore.

Author Contributions

The manuscript was written through contributions of all authors. All authors have given approval to the final version of the manuscript.

Author Contributions

▲These authors contributed equally to this work.

Notes

The authors declare no competing financial interest.

■ ACKNOWLEDGMENTS

This research was supported by Office of Basic Energy Sciences, Department of Energy sp^2 Program (STM instrumentation development and operation) and the SciDAC Program on Excited State Phenomena in Energy Materials funded by the U.S. Department of Energy, Office of Basic Energy Sciences and of Advanced Scientific Computing Research, under Contract No. DE-AC02-05CH11231 at Lawrence Berkeley National Laboratory, and which provided for algorithm and code developments and simulations. Support also provided by National Science Foundation awards no. DMR-1206512 (image analysis) and no. DMR10-1006184 (basic theory and formalism). Computational resources have been provided by the NSF through XSEDE resources at NICS and DOE at NERSC. J.L. acknowledges the National Research Foundation, Prime Minister Office, Singapore, under its Medium Sized Centre Program and CRP award "Novel 2D materials with tailored properties: beyond graphene" (R-144-000-295-281). A.R. acknowledges fellowship support by the Austrian Science Fund (FWF): J3026-N16. STM/STS data were analyzed and rendered using WSxM software.[27]

■ REFERENCES

(1) Mak, K. F.; Lee, C.; Hone, J.; Shan, J.; Heinz, T. F. *Phys. Rev. Lett.* **2010**, *105* (13), 136805.
(2) Han, S. W.; Kwon, H.; Kim, S. K.; Ryu, S.; Yun, W. S.; Kim, D. H.; Hwang, J. H.; Kang, J. S.; Baik, J.; Shin, H. J.; Hong, S. C. *Phys. Rev. B* **2011**, *84* (4), 045409.
(3) Splendiani, A.; Sun, L.; Zhang, Y.; Li, T.; Kim, J.; Chim, C.-Y.; Galli, G.; Wang, F. *Nano Lett.* **2010**, *10* (4), 1271−1275.
(4) Britnell, L.; Ribeiro, R. M.; Eckmann, A.; Jalil, R.; Belle, B. D.; Mishchenko, A.; Kim, Y. J.; Gorbachev, R. V.; Georgiou, T.; Morozov, S. V.; Grigorenko, A. N.; Geim, A. K.; Casiraghi, C.; Neto, A. H. C.; Novoselov, K. S. *Science* **2013**, *340* (6138), 1311−1314.
(5) Zhang, C.; Johnson, A.; Hsu, C.-L.; Li, L.-J.; Shih, C.-K. *Nano Lett.* **2014**, *14* (5), 2443−2447.
(6) Ugeda, M. M.; Bradley, A. J.; Shi, S.-F.; da Jornada, F. H.; Zhang, Y.; Qiu, D. Y.; Ruan, W.; Mo, S.-K.; Hussain, Z.; Shen, Z.-X.; Wang, F.; Louie, S. G.; Crommie, M. F. *Nat. Mater.* **2014**, *13*, 1091−1095.
(7) Wang, H.; Yu, L.; Lee, Y.-H.; Shi, Y.; Hsu, A.; Chin, M. L.; Li, L.-J.; Dubey, M.; Kong, J.; Palacios, T. *Nano Lett.* **2012**, *12* (9), 4674−4680.
(8) Lee, C.-H.; Lee, G.-H.; van der Zande, A. M.; Chen, W.; Li, Y.; Han, M.; Cui, X.; Arefe, G.; Nuckolls, C.; Heinz, T. F.; Guo, J.; Hone, J.; Kim, P. *Nat. Nano* **2014**, *9* (9), 676−681.
(9) Cao, T.; Wang, G.; Han, W.; Ye, H.; Zhu, C.; Shi, J.; Niu, Q.; Tan, P.; Wang, E.; Liu, B.; Feng, J. *Nat. Commun.* **2012**, *3*, 887.
(10) Jones, A. M.; Yu, H.; Ghimire, N. J.; Wu, S.; Aivazian, G.; Ross, J. S.; Zhao, B.; Yan, J.; Mandrus, D. G.; Xiao, D.; Yao, W.; Xu, X. *Nat. Nano* **2013**, *8* (9), 634−638.
(11) Mak, K. F.; He, K.; Shan, J.; Heinz, T. F. *Nat. Nano* **2012**, *7* (8), 494−498.
(12) Mak, K. F.; He, K.; Lee, C.; Lee, G. H.; Hone, J.; Heinz, T. F.; Shan, J. *Nat. Mater.* **2013**, *12* (3), 207−211.
(13) Zeng, H.; Dai, J.; Yao, W.; Xiao, D.; Cui, X. *Nat. Nano* **2012**, *7* (8), 490−493.
(14) Zhang, Y.; Chang, T.-R.; Zhou, B.; Cui, Y.-T.; Yan, H.; Liu, Z.; Schmitt, F.; Lee, J.; Moore, R.; Chen, Y.; Lin, H.; Jeng, H.-T.; Mo, S.-K.; Hussain, Z.; Bansil, A.; Shen, Z.-X. *Nat. Nano* **2014**, *9* (2), 111−115.
(15) Jin, W.; Yeh, P.-C.; Zaki, N.; Zhang, D.; Sadowski, J. T.; Al-Mahboob, A.; van der Zande, A. M.; Chenet, D. A.; Dadap, J. I.; Herman, I. P.; Sutter, P.; Hone, J.; Osgood, R. M. *Phys. Rev. Lett.* **2013**, *111* (10), 106801.
(16) Cheiwchanchamnangij, T.; Lambrecht, W. R. L. *Phys. Rev. B* **2012**, *85* (20), 205302.
(17) Komsa, H.-P.; Krasheninnikov, A. V. *Phys. Rev. B* **2012**, *86* (24), 241201.
(18) Qiu, D. Y.; da Jornada, F. H.; Louie, S. G. *Phys. Rev. Lett.* **2013**, *111* (21), 216805.
(19) Debbichi, L.; Eriksson, O.; Lebègue, S. *Phys. Rev. B* **2014**, *89* (20), 205311.
(20) He, J.; Hummer, K.; Franchini, C. *Phys. Rev. B* **2014**, *89* (7), 075409.
(21) Molina-Sánchez, A.; Sangalli, D.; Hummer, K.; Marini, A.; Wirtz, L. *Phys. Rev. B* **2013**, *88* (4), 045412.
(22) Feenstra, R. M.; Stroscio, J. A. *J. Vac. Sci. Technol. B* **1987**, *5* (4), 923−929.
(23) Hybertsen, M. S.; Louie, S. G. *Phys. Rev. B* **1986**, *34* (8), 5390−5413.
(24) Deslippe, J.; Samsonidze, G.; Strubbe, D. A.; Jain, M.; Cohen, M. L.; Louie, S. G. *Comput. Phys. Commun.* **2012**, *183* (6), 1269−1289.

DOI: 10.1021/acs.nanolett.5b00160
Nano Lett. 2015, 15, 2594−2599

(25) Rohlfing, M.; Louie, S. G. *Phys. Rev. B* **2000**, *62* (8), 4927−4944.
(26) Tersoff, J.; Hamann, D. R. *Phys. Rev. B* **1985**, *31* (2), 805−813.
(27) Horcas, I.; Fernandez, R.; Gomez-Rodriguez, J. M.; Colchero, J.; Gomez-Herrero, J.; Baro, A. M. *Rev. Sci. Instrum.* **2007**, *78* (1), 013705.

DOI: 10.1021/acs.nanolett.5b00160
Nano Lett. 2015, 15, 2594−2599